$\Gamma_8^{(3)}$ resonance in ESR of (ErY)Al_2 single crystals

U. Döbler and K. Baberschke
Institut für Atom- und Festkörperphysik, Freie Universität Berlin, Arnimallee 14, D-1000 Berlin 33, Federal Republic of Germany

S. E. Barnes
Physics Department, University of Miami, Coral Gables, Florida 33124
(Received 18 October 1982; revised manuscript received 2 March 1983)

Angle-dependent ESR results are given for 500-, 2500-, and 5000-ppm Er-doped YAl_2 single crystals. An almost perfect analysis of the X- and Q-band data is achieved if the admixture of the first excited state $\Gamma_8^{(2)}$ into the ground state $\Gamma_8^{(3)}$ via the Zeeman interaction is taken into consideration. This enables us to determine the crystal electric field (CEF) parameter $x=-0.322(20)$ and $W=-0.29(2)$ K. The g-value shift yields $N(E_F)J^{\Delta g}=+0.09(5)$ and the thermal broadening of the linewidth $|N(E_F)J^{\Delta H}|=0.059(5)$. The precision of the experimental data allows, in principle, the determination of a hypothetical anisotropic exchange interaction. However, the fit yields an almost isotropic exchange interaction and upper limits for $|N(E_F)J_4| \lesssim 5\times10^{-5}$ and $|N(E_F)J_6| \lesssim 6\times10^{-8}$. This will be discussed in view of other results, i.e., DyPd. The effect of annealing of local defects on the CEF is discussed. In addition we observe and analyze for the first time the so-called cluster line in a Γ_8 resonance and for high Er concentration. Briefly, we will present similar results on (ErSc)Al_2 single crystals. In addition, we present a detailed theoretical calculation for impurity—conduction-electron and impurity-impurity relaxation for Γ_8 resonances.

I. INTRODUCTION

The crystalline electric field (CEF) splitting of $J=\frac{15}{2}$ rare-earth (RE) ions even in cubic host materials represents a fairly complex problem. Since the Γ_8 representation in the $J=\frac{15}{2}$ manifold and cubic symmetry appears three times, the eigenstates of the quadruplets $\Gamma_8^{(1)}$, $\Gamma_8^{(2)}$, and $\Gamma_8^{(3)}$ depend on the CEF parameters: the prefactors B_4 and B_6 of the Stevens operators[1,2] or the Lea-Leask-Wolf (LLW) parameters x and W.[3] As a consequence of the x-dependent eigenstates, the magnetic moment and its anisotropy change as a function of the CEF parameter. This seems to be the main motivation for the enormous number of experimental investigations of the CEF splitting of RE ions in metals and intermetallic compounds.[4] An attempt to calculate the CEF from first principles in a given matrix was not fully successful on ionic crystals nor in metals.[5]

The experimental techniques divide themselves into two groups: (1) the bulk methods, i.e., specific heat, susceptibility, etc., and (2) resonance methods between CEF levels and their Zeeman levels in an applied field, i.e., inelastic neutron scattering (INS) and ESR.[6] The low excitation energy of ESR (9 GHZ$\cong$0.5 K) limits the ESR to transitions within the ground-state manifold or the very small splitting of S states. Nevertheless, these transitions and their angle dependence can be determined very precisely. In the present investigation we will present results for very low ionic concentrations of Er in YAl_2 single crystals, the angle-dependent resonances in the (110) plane. As a result one gets an almost perfect fit, for the CEF parameters, the g value and the Korringa rate,[7,8] and an upper limit for a hypothetical anisotropic exchange contribution. The latter effect of anisotropic exchange was one motivation for the present work. In recent publications[8] we have shown that for (EuLa)Al_2 and other S-state alloys the general exchange of $a_0\vec{S}\cdot\vec{s}+a_1\vec{L}\cdot\vec{l}$ reduces to its isotropic form since $\langle L_z\rangle=0$ for S states. In contrast, for Er^{3+}, in principle, one should be able to detect both parameters a_0 and a_1.[9] Huang *et al.*[10] have analyzed the DyPd results on that basis.

A second motivation was the clarification of the correct CEF scheme itself. Re ions in the cubic Laves phases have produced an almost infinite number of contradictory results, followed by divergent theoretical interpretations.[11] The result of the present investigation is in fair agreement with recent INS results and yields no concentration dependence

for the CEF splitting from the concentrated $ErAl_2$ down to a few hundreds ppm of Er in Y (and La or Sc)Al_2.[6,12]

The first ESR of Er in YAl_2 was detected by Devine *et al.*[13] They found a single resonance line, which they attributed to a Γ_7 ground state. More recently,[14] we detected the Γ_8 ground state, but still we were not able to determine uniquely the CEF parameters. As a consequence of wrong x and W values, the g-value shift was incorrect as well. But this erroneous determination of the CEF is common in all experimental techniques, i.e., magnetic anisotropy measurements,[15,16] specific heat,[17] magnetization[18,19] and INS.[12,20–22] One reason for the spread of parameters for $ErAl_2$ and its dilutents $ScAl_2$, YAl_2, $LaAl_2$, and $LuAl_2$ may be that the correct x value falls into a regime where the eigenstates are extremely sensitive to x. A similar situation appears occasionally in isolators too, i.e., Nd^{3+} in CaF_2.[23]

In Sec. II we present experimental details. Section III summarizes the theory of the exchange interaction in view of the Γ_8 resonance. In Sec. IV we present and analyze our results. The so-called cluster line in ESR, which is caused by interacting spins, and has been observed quite often for Gd^{3+} and Eu^{2+}, will be reported for the first time in Sec. V for a Γ_8 resonance. Finally, we summarize our experimental work in Sec. VI and compare it with other results. As far as we know the literature, the present work is the first example in which the ESR is able to determine the splitting parameter W via the admixture of the $\Gamma_8^{(2)}$ into the $\Gamma_8^{(3)}$ ground state and one can explain with this admixture the full angle dependence of all transitions.

II. EXPERIMENTAL DETAILS

To study anisotropic effects by means of EPR it is necessary to work with single crystals. In addition, the residual linewidth a is smaller than in polycrystalline samples[24] so that the determination of the field for resonance is more accurate.

The YAl_2 single crystals, doped with 500-, 2500-, and 5000-ppm Er were grown from the melt using the method of Czochralski.[25] The stoichiometric amount of the 99.99%-purity raw materials was molten by an induction furnace and a tungsten crucible under an argon atmosphere of 1.3 bar. Overpressure was used to reduce the evaporation rate of Al, since yttrium and aluminum have different vapor pressures by 2 orders of magnitude. At roughly 1000 °C, Y and Al react exothermically. To get the material homogeneous the temperature of the melt was kept constant well above the melting points of each substance for 10 min. Then the water-cooled tantalum needle was dipped into the melt and pulled up with 5 cm/h. The crucible and the pulling mechanism were rotated with 5 rpm in opposite directions. The single crystals were oriented by the Laue backreflection method and cylindrical samples were cut by "spark cutting," the cylinder axis parallel to the [110] direction. Since the microwaves have a skin depth of the order of 1 μm and spark cutting destroys the surface within a depth of 70 μm all samples were electropolished. The etching solution of 10 ml perclorid acid in 300 ml methanol was cooled down by dry ice to -78 °C to reduce chemical reactivity. To hold this temperature stable the whole apparatus was surrounded by an acetone bath. A stainless-steel plate served as the cathode and the sample as the anode. The applied voltage was roughly 50 V and the current 1 A. As a minimum a layer of $\frac{1}{10}$ mm thickness was removed. This method has the advantage that all elements of the intermetallic compound are etched equally, since the applied voltage of 50 V is very much larger than the differences in the chemical potentials, which could yield a selective etching.

To reduce crystalline defects all samples were annealed. They were wrapped in an evaporated tantalum foil and put into a quartz tube under an argon atmosphere. The annealing temperature was 800 °C and the time 12 and 24 h. The residual linewidth in the EPR experiments has been reduced by annealing by more than a factor of 2 (see Fig. 9 and Sec. IV). No further improvement was detectable by 24 h annealing.

All samples were checked on grains with a microscope and point by point on the whole surface with the Laue x-ray diffraction method. Although x rays have a penetration depth of only $\frac{1}{100}$ mm one can be sure that the bulk is homogeneous single crystalline if the Laue pattern remains the same after rotating the sample by 180°. A further criterion for the quality of the crystal is the sharpness of the Laue spots. With sharp spots and a sample film distance of 5 cm the spread in orientation of a hypothetical mosaic structure is less than $\frac{1}{2}$°. The EPR line shape, intensity and residual linewidth yield information about the quality of the crystal.

The EPR measurements were performed with a Varian E line EPR spectrometer at microwave frequencies of 9.5 and 35 GHz. The sample was cooled in a helium-bath Dewar and the temperature varied from 4.2 to 1.2 K. The magnetic field was rotated in the (110) plane, and $\theta=0°$ corresponds to the [100] direction. A possible tilt angle from the rotation axis to the [110] direction is less than 2°.

III. THEORY

One of our prime objectives in undertaking this work was to provide, if possible, conclusive evidence

in favor of an anisotropic exchange.[9] In the following discussion we estimate the magnitude of the *anisotropic exchange* for our experiment and then ask why it has been tentatively observed in other systems but not in our system.

In agreement with many authors[9,10] we take as a model one in which the principal interaction is between the $4f$ and $5d$ electrons on the impurity site. However, since the electronic structure of Y is very similar to that of Gd we assume, for the present purposes, that the $5d$ density on the impurity site is the same as elsewhere in the crystal. Since the values of these exchange integrals are known, it should be possible to evaluate directly the exchange parameters for our experiment. This is known not to work; the bare calculated values are perhaps three times too large. This discrepancy has been explained in terms of the antiferromagnetic Kondo effect.[8]

The lowest two terms in the anisotropic exchange are

$$\mathcal{H}_1 = -a_0 \vec{S}\cdot\vec{s} - a_1 \vec{L}\cdot\vec{l} \ ,$$

where $a_0 \cong 0.4$ eV and $a_1 \cong 0.016$ eV.[8] If we assume that the conduction electrons are in thermal equilibrium we may replace $\vec{s}$ and $\vec{l}$ by their expectation values.

With the field in the z direction

$$\mathcal{H}_1 = -a_0 S_z \langle s_z \rangle - a_1 L_z \langle l_z \rangle \ .$$

By definition $-g_e \mu_B \langle S_z \rangle = \chi_{sp} H_0$ and $-\mu_B \langle l_z \rangle = \chi_{ob} H_0$, where χ_{sp} and χ_{ob} are the spin and orbital contributions to the $5d$ susceptibility. With this

$$\mathcal{H}_1 = a_0 \left[\frac{\chi_{sp}}{\mu_B}\right] S_z H_0 + a_1 \left[\frac{\chi_{ob}}{\mu_B}\right] L_z H_0$$

$$= \left[(g_{J-1}) a_0 \left[\frac{\chi_{sp}}{\mu_B^2}\right] + (2-g_J) a_1 \left[\frac{\chi_{ob}}{\mu_B^2}\right] \right] J_z H_0$$

$$\equiv J_{eff} J_z H_0 \ .$$

With $g_J = \frac{6}{5}$ for Er and the above for a_1 and a_0 we find that the ratio of the first to second contribution to J_{eff} is $\chi_{ob}/7\chi_{sp}$, typically small but not negligible.

Finally we ask, what is the relationship of (ErY)Al_2 to other systems for which there does seem to be evidence for an anisotropic exchange (Table IV)? If one accepts the analysis of this system as correct, Er*Pt* (Ref. 26) is particularly striking. The Γ_6 ground state has a negative g-value shift from the nominal $g=6$ while the resonance lines of the Γ_8 excited state are shifted to lower field, corresponding to a positive g-value shift. Both these shifts can be reconsidered with the given anisotropic exchange but clearly not with an isotropic exchange which would shift both the Γ_6 and Γ_8 in the same direction. The evident difference between Dy*Pd*,[26-28] Er*Pd*,[26,29,30] Dy*Pt*,[26] Er*Pt*,[26] and (ErY)Al_2 is the negative value of this isotropic component of the exchange which may (or may not) be linked to covalency. If one does accept the covalent explanation for the negative exchange in the anisotropic systems, then we must use an entirely different model to calculate the ratio of J_4/J_0. The matrix elements in the covalent exchange which involve changes in the angular momentum of the ion are as large as those which do not, and consequently one should expect a detectable anisotropic exchange. This point needs further investigation.

Now we turn to the calculation of the *resonance fields* H_{res}. Following the preceding paragraphs and for a single ion, we have to add to $\mathcal{H}_{CEF}$ (Ref. 2) and $\mathcal{H}_{Zeeman}$ (Ref. 2) the exchange Hamiltonian $\mathcal{H}_{ex}$ (Ref. 28),

$$\mathcal{H}_{CEF} = W[xO_4(J)F^{-1}(4) + (1-|x|)O_6(J)F^{-1}(6)] \ , \quad (1)$$

$$\mathcal{H}_{Zeeman} = \mu_B g_J \vec{J}\cdot\vec{H} \ , \quad (2)$$

$$\mathcal{H}_{ex} = [J_0 + J_4 O_4(L) + J_6 O_6(L)] \mu_B N(E_F) \vec{S}\cdot\vec{H} \ . \quad (3)$$

The hyperfine interaction will be included later on as a small perturbation.

The diagonalization of Eq. (1) plus Eq. (2) yields the eigenvalues and eigenstates in $|J,J_z\rangle$ representation. In order to include Eq. (3), which is a function of the angular momentum $\vec{L}$, one has to choose the eigenstates in the $\vec{L}$ and $\vec{S}$ representation using the appropriate Clebsch-Gordan coefficients.[31]

Figures 1 and 2 show the corresponding LLW diagram and the Zeeman splitting of the two lowest Γ_8's, respectively. We label the eigenstates with $|\alpha_1\rangle$, $\alpha_i = 1,2,3,4,5$, etc., starting from the bottom. Figure 2 demonstrates the influence of the $\Gamma_8^{(2)}$ on the $\Gamma_8^{(3)}$ (and vice versa) for Q-band experiments. The dashed lines are for isolated quadruplets. At X band this admixture is too small to be detected.

The *relaxation dynamics* of the Γ_8 is more complex. It has been developed recently.[7] Assuming that the bottleneck is not relevant to a Γ_8 resonance, the equation of motion for the local-moment density matrix for the ground manifold is

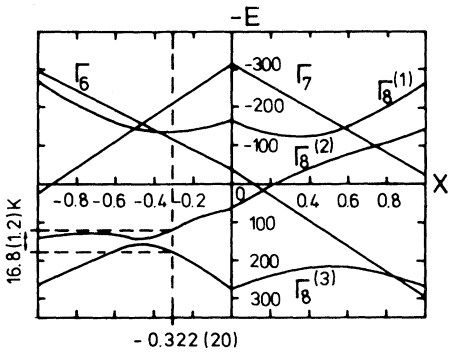

FIG. 1. Lea, Leask, and Wolf diagram for $J=\frac{15}{2}$ (Ref. 3). W has been chosen to be negative. The vertical and horizontal dashed lines indicate the results of this work.

$$\frac{d}{dt}\rho_s = i[\rho_s,\mathscr{H}_s] - \frac{1}{2T_{se}}[\vec{J},[\vec{J},\delta\rho_s]] - \frac{1}{T_{sL}}\delta\rho_s \ , \tag{4}$$

where $\delta\rho_s$ is the instantaneous deviation from equilibrium

$$\delta\rho_s = [\rho_s + (\mathscr{H}_s/ZkT)] \ , \tag{5}$$

and where $\mathscr{H}_s$ is the molecular field plus crystal field Hamiltonian,

$$\mathscr{H}_s = g_J\mu_B\vec{J}\cdot(\vec{H}_{\rm ext}+\lambda\vec{M}_e+\alpha\vec{M}_s)+\mathscr{H}_{\rm CEF} \ . \tag{6}$$

The other quantities are

$$1/T_{se} = \pi[(g_J-1)N(E_F)J^{\Delta H}]^2kT \ ,$$

which is the Korringa rate, $1/T_{sL}$, which is the residual width assumed to be temperature independent, and λ, in Eq. (6), which is the same for each transition; our experiments suggest that the latter is not true. We shall adapt for this later in the analysis. Finally, Z is the partition function.

While the presence of excited crystal-field levels is important to an accurate determination of the field for resonance it is not so for relaxation effects, at least in our limited temperature interval (1.2–4.2 K), and so we make the isolated Γ_8 approximation of replacing $\vec{J}$ by $(\vec{V}g_J)$. The description in the $|J,J_z\rangle$ manifold does not need higher-order terms as J^3, unlike the effective spin model in Ref. 2. Note that the levels 1 and 3 as well as 2 and 4 are Kramers conjugates denoted by $|3\rangle=|\bar{1}\rangle$ and $|4\rangle=|\bar{2}\rangle$.

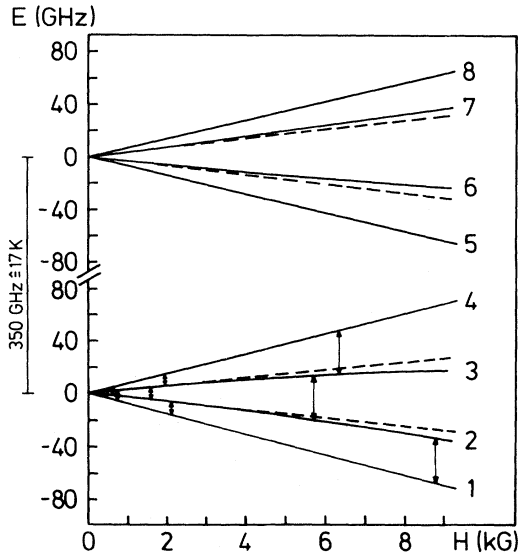

FIG. 2. Energy as a function of the applied magnetic field H for the $\Gamma_8^{(3)}$ ground state and the first excited level $\Gamma_8^{(2)}$. $x=-0.322$, $W=-0.29$ K and are parallel to [100] axis ($\theta=0°$). The actual spectra for X band (0–2 kG) and Q band (5–9 kG) are shown in Figs. 10 and 3, respectively. The dashed lines indicate $E(H)$ for the isolated Γ_8 ($W\to\infty$).

The general equation of motion is

$$\frac{d}{dt}\rho_{\alpha\beta} = \left[i(\beta-\alpha)-\frac{1}{\tau_{\alpha\beta}}-\frac{1}{T_{sL}}\right]\delta\rho_{\alpha\beta} + \sum_{\gamma,\sigma}\frac{1}{\tau_{\alpha\beta\gamma\sigma}}\delta\rho_{\gamma\sigma} \ , \tag{7a}$$

where

$$\frac{1}{\tau_{\alpha\beta}} = dT[(\langle\alpha|V_z|\alpha\rangle-\langle\beta|V_z|\beta\rangle)^2+\tfrac{1}{2}(\langle\alpha|V_+|\alpha\rangle-\langle\beta|V_+|\beta\rangle)^2+\tfrac{1}{2}(\langle\alpha|V_-|\alpha\rangle-\langle\beta|V_-|\beta\rangle)^2] + \tfrac{1}{2}dT\sum_{\xi=1}^{4}|\langle\alpha|V_+|\xi\rangle|^2+|\langle\alpha|V_-|\xi\rangle|^2+\tfrac{1}{2}dT\sum_{\xi=1}^{4}|\langle\beta|V_+|\xi\rangle|^2+|\langle\beta|V_-|\xi\rangle|^2 \tag{7b}$$

and

$$d = \frac{\pi}{2\hbar}\left[\frac{g_J-1}{g_J}N(E_F)J^{\Delta H}\right]^2 k \ .$$

The second and third terms in the sum are not given in previous calculations [Eq. (3.16) in Ref. 7]. They become relevant in the present experiment because we are able to determine the relaxation for $\theta \neq 0$.

The following term for $1/\tau_{\alpha\beta\gamma\sigma}$ again becomes important only for the 1—2 and 3—4 transitions and $\theta \neq 0$:

$$\frac{1}{\tau_{\alpha\beta\gamma\sigma}} = dT(2\langle\gamma|V_z|\alpha\rangle\langle\sigma|V_z|\beta\rangle + \langle\gamma|V_+|\alpha\rangle\langle\sigma|V_+|\beta\rangle + \langle\gamma|V_-|\alpha\rangle\langle\sigma|V_-|\beta\rangle) \tag{7c}$$

in agreement with the results of Sy and Walker[32] that these degenerate transitions give a single resonance with a relaxation rate

$$\frac{1}{\tau} = \frac{1}{\tau_{\alpha\beta}} - \frac{1}{\tau_{\alpha\beta\bar{\beta}\bar{\alpha}}} + \frac{1}{T_{sL}} . \tag{8}$$

However, when the two transitions are separated such that

$$|(\beta-\alpha)-(\bar{\alpha}-\bar{\beta})| > (1/\tau_{\alpha\beta\bar{\beta}\bar{\alpha}}) ,$$

Eq. (7) applies and they give separate resonances at $\beta-\alpha$ and $\bar{\alpha}-\bar{\beta}$ both with a rate

$$\frac{1}{\tau} = \frac{1}{\tau_{\alpha\beta}} + \frac{1}{T_{sL}} . \tag{9}$$

The relaxation rate $1/\tau_{\alpha\beta\bar{\beta}\bar{\alpha}}$ tends to narrow the two resonances and will do so if the inverse of the above inequality is satisfied. Then the width reverts to that given by Eq. (8) at a resonance frequency given by the simple average of $\beta-\alpha$ and $\bar{\alpha}-\bar{\beta}$.

Thus the discussion of the theory of a Γ_8 with nonoverlapping resonances is concluded, that is, for high frequency (Q band) and small concentrations. We shall present data for a lower frequency (X band) and rather large concentrations (5000 ppm) for which the resonances do overlap. For this case the other rates $1/\tau_{\alpha\beta\gamma\sigma}$ become important.

The size of the matrix elements which determine these rates depends very much upon the Γ_8 involved (i.e., the values of x and W). For our Γ_8 ground manifold there are equal couplings between the pairs $1\rightarrow 2$ and $\bar{2}\rightarrow\bar{1}$ to the transition $2\rightarrow\bar{2}$ with (as noted above) no coupling directly between. This much is a consequence of symmetry. What is perhaps unique here is that the matrix element $\langle\bar{1}|V_+|\bar{2}\rangle = \langle 2|V_+|1\rangle$ is also approximately equal to the matrix element $\langle\bar{2}|V_+|2\rangle$, while the other symmetry-allowed matrix element $\langle\bar{1}|V_+|1\rangle$ is negligible. As a consequence, the intensities of the various lines, their relaxation rates, and cross-relaxation rates are all roughly equal to each other, with relaxation rates of $\cong 50$ G/K. The relaxation paths are illustrated in Fig. 2. The situation is almost identical to that considered in the exchange motional theory developed for fine structure of S-state resonances. For X band, upon raising the temperature the $1\rightarrow 2$ and $\bar{2}\rightarrow\bar{1}$ pairs on the one hand and the $2\rightarrow\bar{2}$ transition on the other should draw together into a single resonance near the center of gravity.

The other relaxation phenomenon we wish to discuss is the formation of a cluster resonance due to cross relaxation between different ions in higher concentrations and lower frequencies. As shown by Hardiman *et al.*,[33] this relaxation is additive to the rates $1/\tau_{\alpha\beta}$ and $1/\tau_{\alpha\beta\gamma\sigma}$. In particular, for $\theta=0°$ and in the present notation the thermal broadening bT is replaced by

$$bT + \left[\frac{kT}{4\omega}\right] \sum_{\substack{i,j \\ j\neq i}} (J_{ij})^2 \mathrm{Im}[\chi_j^+(\omega+is)] , \tag{10}$$

where J_{ij} is the strength of the Ruderman-Kittel-Kasuya-Yoshida (RKKY) interaction between the ions,

$$\mathscr{H}_{ss} = -\sum_{i<j} J_{ij} \vec{V}_i \cdot \vec{V}_j ,$$

and $\chi_j^+(\omega+is)$ is the transverse dynamic susceptibility of the jth ion. The sum is over all ions except the one in question. Clearly, in a random alloy, this sum has a statistical nature. Its magnitude will vary from ion to ion with the result that, under favorable conditions, some ions will be motionally narrowed by the processes described above while others will not, the former ions of course generating the cluster resonance.

IV. RESULTS AND ANALYSIS

Figure 3 shows the angle-dependent spectra for the 500-ppm sample. The 1—2 and 2—3 transitions are detected for the full range of angles in the (110) plane (Fig. 4). In addition, the 3—4 transition is detected in a small range of angles close to the [100] direction. This additional line, which should not appear separately in an isolated Γ_8 resonance, is the key for a unique interpretation of the spectra. It was missing in our previous experiment.[14] The dashed line in Fig. 3 shows the fit spectrum. We used for each transition a perfect Dysonian line shape ($A/B=2.53$). The dashed-dotted lines at $\theta=30°$ and 90° are the individual lines, which are superposed to the dashed one. In Fig. 5 we added for the [111] direction the hyperfine interaction as a

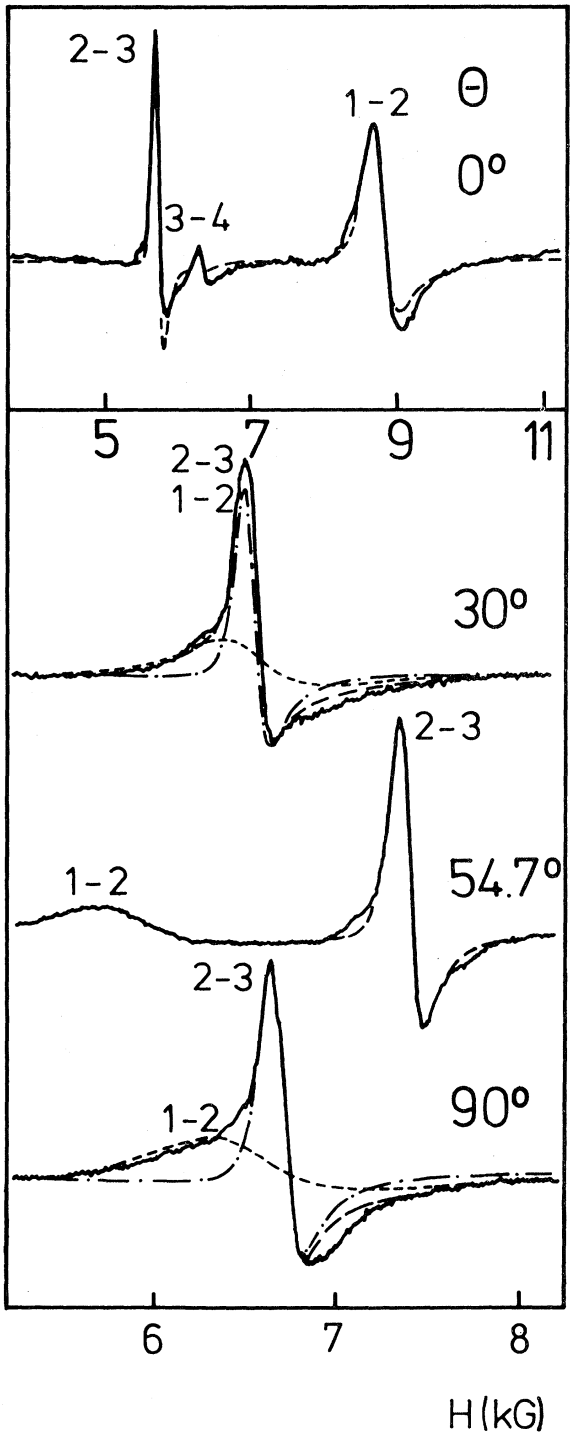

FIG. 3. Q-band spectra for 34.61 GHz, $T=1.25$ K, and $c=500$ ppm. The dashed and dashed-dotted lines represent our best fit of the single lines and the superposition.

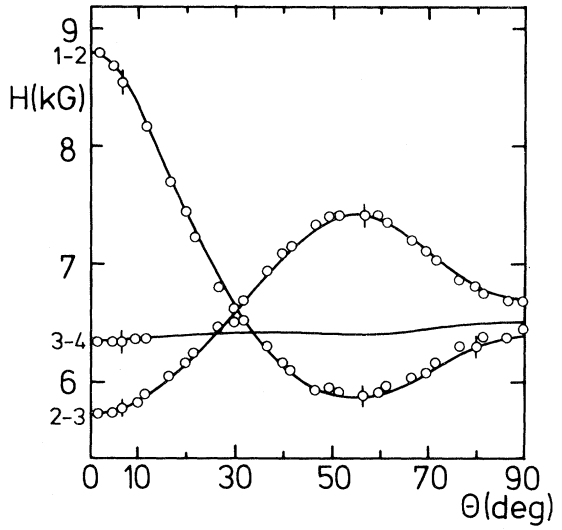

FIG. 4. Resonance field as a function of orientation, θ being the angle between $\vec{H}$ and [100] in the (110) plane. The solid line is our best fit with $x=-0.322$, $W=-0.29$ K, and $N(E_F)J^{\Delta g}=+0.09$.

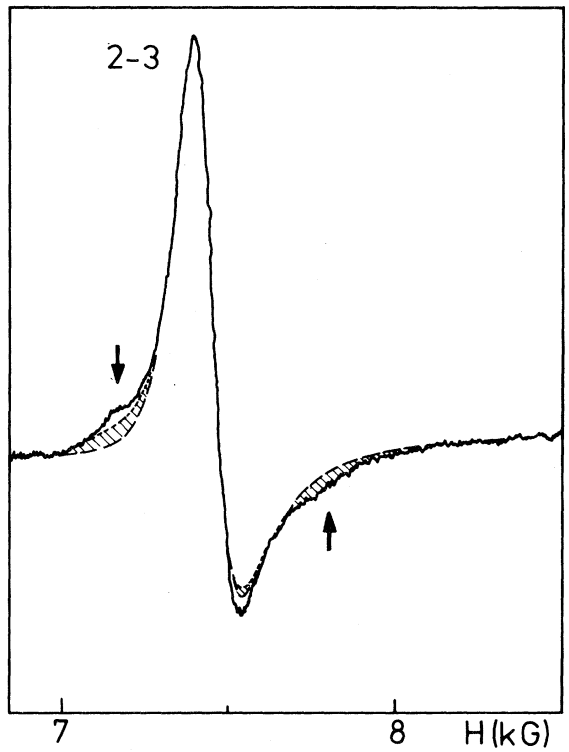

FIG. 5. Same spectrum as in Fig. 3 at $\theta=54.7°$, but the fit encloses the hyperfine interactions. The shadowed regimes indicate the additional intensities, the arrows the outermost positions of the hyperfine resonance fields.

small perturbation into the fitting procedure. In second-order perturbation theory one gets for the 2—3 transition

$$H_{\rm res}=H_0+AM_I-(A^2/2H_0)[I(I+1)-M_I^2]\ .$$

H_0 is the resonance for the 77% of isotopes with $I=0$. For the 23% of ^{167}Er the signal intensities of each of the eight lines was chosen according to the relative abundance. The linewidth ΔH was the same as for the central $I=0$ line. For A we choose $A=-75.5$ G.[34]

From Figs. 3 and 5 one sees that the fit and the experiment agree almost perfectly. Again, we would like to emphasize that we kept the line shape fixed, that is to say, a Lorentzian absorption shape plus its dispersion. In the early time of sample preparation for ESR in metals the signals were much broader due to inhomogeneous broadening.[13] In those cases quite often the A/B ratio was varied to get a better fit. That is to our opinion unphysical and yields incorrect resonance fields.[35]

Our error bars are given in Fig. 4. The solid line yields the best fit by diagonalizing Eqs. (1) and (2) and taking x and W as free parameters. The sensitivity of $H_{\rm res}(\theta)$ with respect to x, W is shown in Fig. 6. For a very large CEF splitting ($W=100$ K) one yields two transitions, the Kramers conjugate 1—2 and 3—4 coincide. A variation of x changes

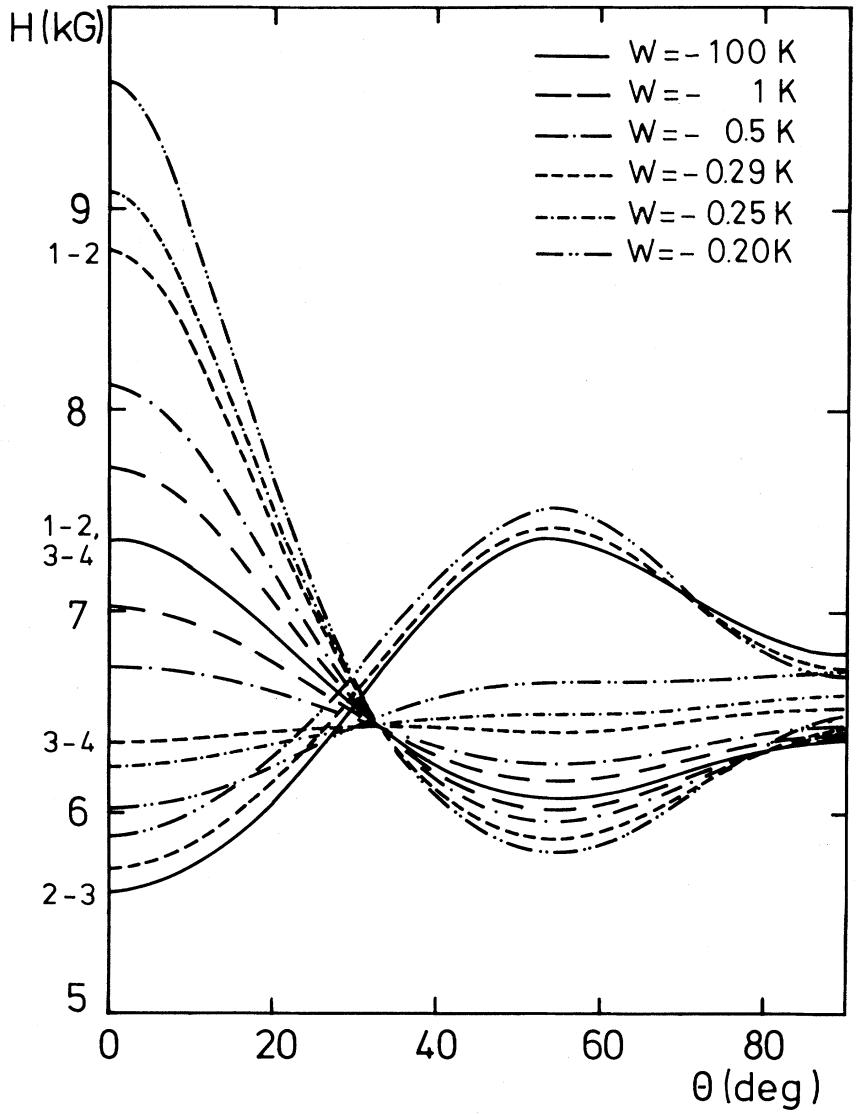

FIG. 6. Computer simulation of the resonance fields according to Eqs. (1)—(3) for variable W parameter and fixed $x=-0.322$ and $N(E_F)J^{\Delta g}=+0.09$. The microwave frequency equals $\nu=34.61$ GHz.

the center of gravity for $H_{res}(\theta)$. For small CEF splitting ($W \approx -0.3$ K) $H_{res}(\theta=0)$ changes dramatically for the 1—2 and 3—4 transitions. This enables us to determine the CEF splitting precisely to be $W=-0.29(2)$ K and $x=-0.322(20)$. Again, in general the ESR in the ground-state manifold does not yield the W parameter but only x. For $(ErY)Al_2$, accidentally the small splitting between $\Gamma_8^{(2)}$ and $\Gamma_8^{(3)}$ enables us to determine both.

So far we did not include the exchange interaction in the discussion. The actual fit for Fig. 4 has been performed taking the Knight shift also into consideration. Since the amount of shift depends on the applied field and and the field ranges from 5.8 to 7.5 kG for the 2—3 transition, the $|\frac{1}{2}\rangle - |-\frac{1}{2}\rangle$ transition in the isolated Γ_8 notation and from approximately 2—6 kG for the 1—2 transition, a quite precise determination of a phenomenological exchange strength, is possible yielding $N(E_F)J^{\Delta g} = +0.09(5)$.[35] We will come back to this point and the discussion of anisotropic exchange at the end of this section.

The integrated intensities of each transition and for different orientations θ give a crosscheck for the energy scheme discussed above (Fig. 2). The theoretical values of the intensity in Table I were calculated by taking into account (i) the actual wave function for the transition probability and (ii) the appropriate Boltzmann factors. The experimental values were taken from the fit curve.[36] The agreement is fairly good. The different intensities between the 1—2 and 3—4 transitions are essentially due to the Boltzmann factor and in reasonable agreement with the experiment. One uncertainty in the experimental intensity is the unknown inhomogeneous contribution of the linewidth.

Figure 2 also shows the transitions for the X band. We have recorded those spectra as well but for the present discussion they are less important, because the Zeeman interaction is too small for a significant admixture. We will come back to these data in the cluster discussion (Sec. V).

In Figs. 7 and 8 we have plotted the linewidth $\Delta H(T,\theta)$ as a function of temperature. The 2—3 transition shows the most narrow width and a small (almost zero) residual linewidth a. According to the different matrix elements in Eq. (7b) the thermal broadening changes as a function of orientation. From Eq. (7b) one expected a relative change in the slope for $\theta=0°$, 54.7°, and 90° of 1, 0.72, and 0.66, respectively. The experimental values are 60, 65, and 40 in agreement with theory but are not very significant because of the large experimental error bars. The comparison between theory and Fig. 8 agrees qualitatively too. The relative change of the matrix elements for the three transitions 2—3, 3—4, and 1—2, and $\theta=0°$, is 1, 0.76, and 0.71 and experimentally 60, 55, and 54. Thus, the exchange coupling can be determined consistently from all the thermal broadening slopes. We get $|N(E_F)J^{\Delta H}| = 0.059(5)$.[37]

Finally, we wish to analyze the residual linewidth a. It yields helpful information on the microscopic CEF symmetry at the Er impurity site. It is well known from insulator physics (see p. 729 in Ref. 2) that the 2—3 transition—a Kramers doublet—is relatively insensitive to local distortions. On the other hand, the 1—2 and 3—4 transitions are affected in first order by local distortions. A random distribution of strain, therefore, will broaden inhomogeneously the later transitions, in exact agreement with experiment. Moreover, one can calculate the "sensitivity" of the different H_{res} (1—2 and 3—4) on the CEF parameters—that is to say the derivative $\partial H_{res}/\partial x$ and $\partial H_{res}/\partial W$ at $x=-0.322$ and $W=-0.29$ K.[38] For both derivatives the values for 1—2 are two times larger than for 3—4. This qualitatively good agreement between the $T=0$ intercepts in Fig. 8 and the theoretical interpretation is promoted by an additional experiment we did on nonannealed single crystals. Figure 9 shows the ESR of the same single crystal before and after annealing (Sec. II). It is obvious how annealing reduces internal strain and produces more narrow

TABLE I. Thermal broadening b, residual linewidth a, and intensities for the different transitions and angles (see Figs. 7 and 8). The intensities are normalized to $\theta=0°$; the experimental values represent the integrated intensities.

θ	Transition	b(G/K)	a(G)	Intensity Theoretical	Intensity Experiment
0°	2—6	60(15)	0	1	1
0°	3—4	55(20)	55	0.2	0.2
0°	1—2	54(25)	213	2.9	6.3
0°	2—3	60(15)	0		
54.7°	2—3	65(15)	22		
90°	2—3	40(20)	77		

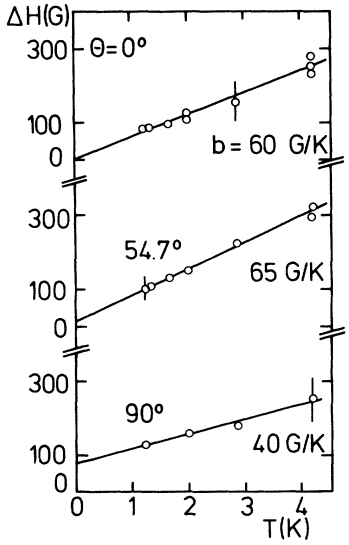

FIG. 7. Temperature dependence of the 2—3 transition from Fig. 3. For error bars of the thermal broadening b see Table I.

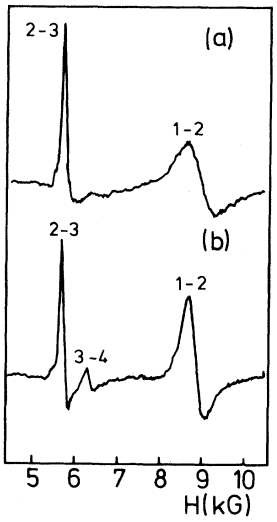

FIG. 9. ESR spectrum for different sample quality. $c=500$ ppm, $\nu=34.61$, $\theta=0°$; (a) $T=1.25$ K nonannealed, (b) $T=1.7$ K annealed (see Sec. II). The latter spectrum has been taken at 1.7 K because the 3—4 transition becomes weaker at lower temperature.

and Dyson-type lines. It is worthwhile to mention that ESR is a very sensitive tool[24] to study local environment and symmetry.

In the next paragraph we will discuss the analysis of anisotropic exchange. So far we have reported on experimentally determined exchange interaction from the g-value shift and the linewidth, respectively. The relaxation data do have too large error bars for extracting higher-order terms in the exchange.

For the full analysis of H_{res} we take Eq. (3) seriously in our fit program, namely, we introduce three independent parameters J_0, J_4, and J_6 instead of one phenomenological $J^{\Delta g}$. The question arises as to how significant J_4 and J_6 are. In short, the matrix elements of $O_4(L)$ and $O_6(L)$, respectively, change H_{res} in the following way: Positive J_4 reduces the resonance field at $\theta=0°$ for the 1—2 transition and has almost no effect on the 3—4 and 2—3 transitions. At $\theta=54.7°$, 1—2 is not affected, but H_{res} (2—3) is reduced. J_6 acts more or less isotropically (for all transitions equally). Consequently, there are cross plays between J_6 and J_0 as well as between J_4 and W. This problem and the weakness of an hypothetical anisotropic exchange make a precise determination of J_0, J_4, and J_6 difficult. On the one side we are able to fit all experimental data (X band included), in particular Fig. 4, with an isotropic exchange. In this case J_0 is identical to $J^{\Delta g}$. This fit is excellent and the precision of the individual data points is better than in other ESR work—due to the narrow lines in this experiment. If, on the other hand, we force our program for finite J_4 and J_6 we end with an upper limit of $|N(E_F)J_4| \approx 5\times10^{-5}$ and $|N(E_F)J_6| \approx 6\times10^{-8}$.

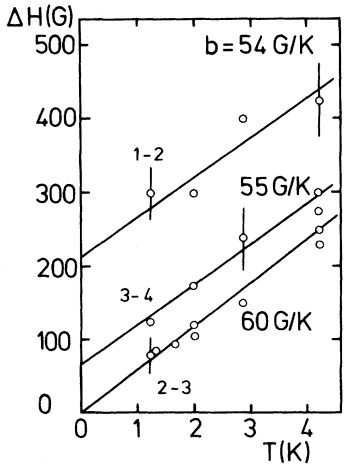

FIG. 8. Same as Fig. 7 but for all three transitions and $\theta=0°$.

V. Er-Er INTERACTIONS

At a first view the difference of the X-band spectra (Figs. 10—12) in contrast to the Q-band spectra for $\theta=0°$ is the observation of more resonance lines. At the low-field side two transitions 1—3 and 2—4 occur. They are forbidden in a Γ_8 manifold, even in the case of admixtures of an excited $\Gamma_8^{(2)}$ via Zeeman

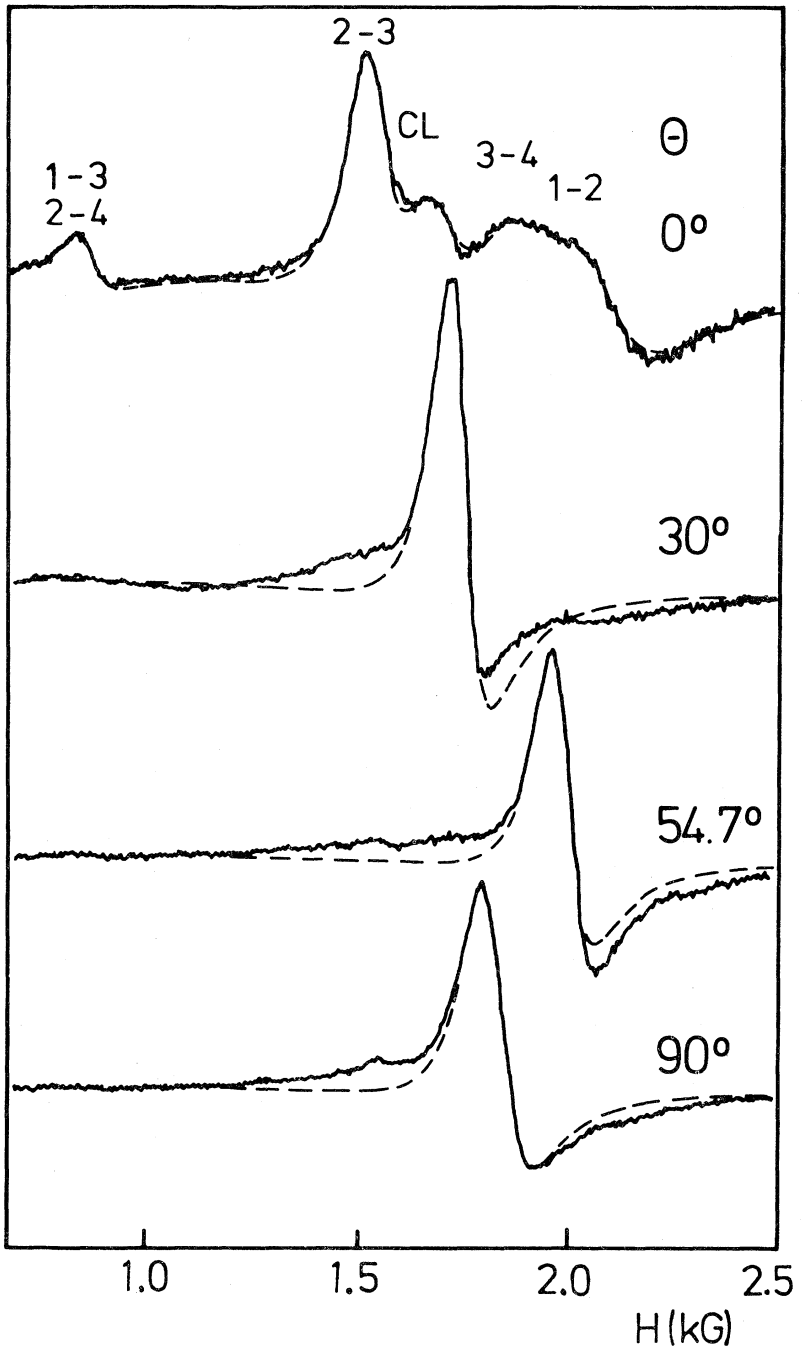

FIG. 10. X-band spectra $\nu=9.36$ GHz, $c=500$ ppm, and $T=1.3$ K. The dashed line is the sum of the single-ion fit (see Sec. IV) taking the same CEF and exchange parameters as for Q band (see Fig. 3) and the additional "cluster line."

interaction. Figure 11 shows clearly a concentration dependence of the intensity of these transitions. Furthermore, an additional line (CL) exists which cannot be interpreted as a transition within the Γ_8 manifold. Also, this line is concentration dependent and it may be that the intensity variations of the 1—3 and 2—4 transitions are correlated with the existence of the extra "cluster" line. Figure 11 shows for the 500- and 2500-ppm spectra a decomposition of the transitions within the Γ_8 manifold and the cluster line. The cluster line contains about 25% for 500 ppm and 40% for 2500 ppm of the total intensi-

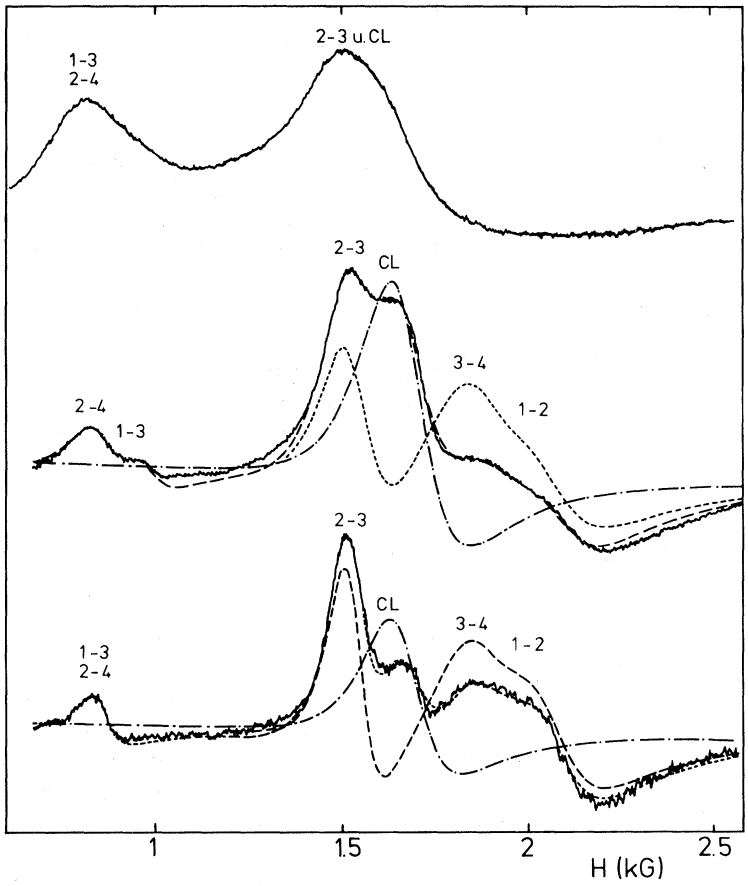

FIG. 11. X-band spectra for different concentrations (ppm), $\theta=0°$, $T=1.3$ K. The dashed-dotted line represents the cluster line (Sec. V); here the linewidth and position are free parameters: $\Delta H=150$ G, $H_{res}=1680$ G, and $A/B=2.53$. The short dashed line is the single-ion fit and the long dashed line is the superposition.

ty and lies roughly midway between the 2—3 transition and the 3—4 and 1—2 pair.

To our knowledge, this is the first observation of such a cluster line in any system other than for the S-state ions Gd^{3+} and Eu^{2+} in hosts where they exhibit fine structure. The phenomena observed here and in the S-state systems are remarkably similar.[7,39,40] As here, the S-state *cluster lines when present at X band are invariably absent at Q band.* Compare Figs. 10 and 3; they are recorded for the same 500-ppm sample roughly at the same temperature but at different frequencies. Also, as here, the intensity of the cluster when present grows with increasing temperature (Fig. 12). For this reason we believe it is reasonable to interpret the two phenomena in the same terms, namely, using the theory of ion-ion cross relaxation introduced in Sec. III. We note again that a similar process does not occur for hyperfine structure and indeed a cluster line has never been observed in hyperfine structure.

A brief discussion of the deceptively innocent looking Eq. (10) (Sec. III) should convince the reader that the detailed calculation of the cluster resonance signal is not at all simple. The problem lies in the self-consistent calculation of the local susceptibility $\chi_j^+(\omega)$ together with the random nature of the sum over ions. The problem is similar in complexity but different in physical content to the calculation of the internal field distribution in a spin-glass.[40] We therefore restrict ourselves to a crude estimate of the internal ion-ion fields involved and a brief discussion of our understanding of the above-mentioned phenomena.

First, we estimate the magnitude of the rms field $[(J_{ij})^2]^{1/2}$ by calculating the spin-spin interaction necessary to narrow two ions into the cluster resonance by mutual spin-spin cross relaxation. For the local susceptibility we write

$$\chi_j^+(\omega)=(\omega_s-i\Delta)(\omega_s-i\Delta-\omega)\ ,$$

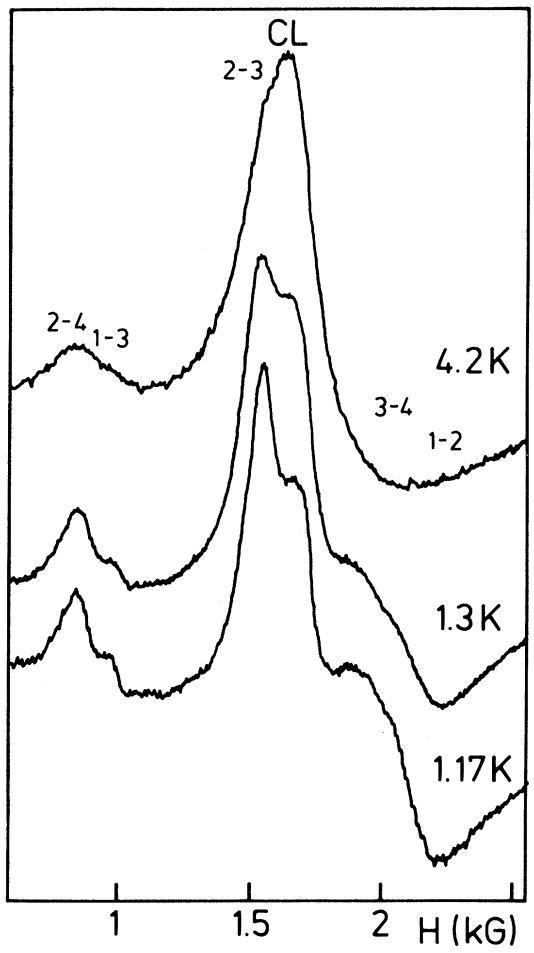

FIG. 12. Temperature dependence for the 2500-ppm single crystal. $\nu=9.36$ GHz.

where ω_s is the cluster resonant field and Δ its width. One has

$$\mathrm{Im}\chi_j(\omega_0+is)=\chi_s^0\omega/\Delta\ .$$

We take $\Delta\cong 100$ G, calculate χ_s^0 in the standard way, and take 500 G as an estimate for the separation $|(\beta-\alpha)-(\gamma-\sigma)|$ of the 2–3 pair from the 1–2 and 3–4 pairs (Fig. 10).

The result is $J_{ij}\sim\pm 40$ G. However, this estimate of the interaction should be treated as an upper bound. We reason as follows: With 30% of the ions contributing to the cluster one might begin by assuming that 15% of the J_{ij} exceed our estimate of 40 G. However, this is a typical perculation concentration, hence most ions will be connected to more than one ion if the concentration of such bands is 15%. In addition, one notices that ions need not narrow in pairs. There is considerable intensity of the 2–3, 1–2, and 3–4 resonances at the cluster position and hence a correspondingly relatively large value of $\mathrm{Im}\chi_j$ at this point for ions not in the cluster. Taking both considerations together we suggest at least initially that when it is of low relative intensity the cluster is not formed out of pairs but rather simply from single ions interacting with the nonclustered ions. This interaction is larger for the cluster ions because of the statistical nature of the sum $\sum_j (J_{ij})^2\chi_j$.

Clearly, as would be any sensible theory for the cluster resonance, the explanation is consistent with the concentration dependence of cluster intensity and the linewidths in general; the higher the concentration the larger is the sum $\sum_j (J_{ij})^2\chi_j$, and thereby the cross relaxation, the linewidths of the nonnarrowed lines (involving a sum of Korringa and cross-relaxation), and the cluster intensity. In addition, the more subtle relationship between the cluster frequency and temperature can be understood. To have an appreciable cluster resonance requires an appreciable intensity of the point, somewhere in the middle of the spectrum where the cluster will form. There is no cluster while a cluster does form for the same sample at X band where such an intensity exists.

The variation with temperature is more interesting. One should compare the 2500-ppm X-band data with that for the S-state system, LaSb:Gd^{3+}.[41] At the lowest temperatures this latter system shows a well-resolved fine structure without a cluster. A

TABLE II. CEF parameter for Er in the cubic dialuminum Laves phase.

System	Conc.	x	W(K)	Technique	Ref.
$ErAl_2$	100%	−0.26	−0.29	magnetization	19
(Er*Y*)Al_2	20%	−0.30	−0.25	INS	21
(Er*Y*)Al_2	2%	−0.30(2)	−0.25(2)	INS	12
(Er*Y*)Al_2	5000 ppm	−0.30	−0.25	magnetic anisotropy	15
(Er*Y*)Al_2	500 ppm	−0.322(20)	−0.29(2)	ESR	This work
(Er*Sc*)Al_2	500 ppm	$\approx$ −0.2	$\approx$ −0.3	ESR	This work
(Er*Sc*)Al_2	2%	−0.20	−0.26	INS	12
(Er*La*)Al_2	2%	−0.48	−0.18	INS	12

TABLE III. Exchange-coupling strength from g-value shift and relaxation. The different figure of $N(E_F)J^{\Delta H}$ in the third row and in Ref. 14 is due to a different definition (factor $\sqrt{2}$) in Ref. 32 and the present one in Ref. 7.

System	$N(E_F)J^{\Delta g}$	$N(E_F)J^{\Delta H}$	Technique	Ref.
(Gd*Y*)Al_2	+ 0.07	0.046	ESR	43
(Gd*Lu*)Al_2	+ 0.085	0.056	ESR	43
(Er*Y*)Al_2	+ 0.52	0.065(7)	ESR	14
(Er*Y*)Al_2	+ 0.09(5)	0.059(5)	ESR	This work
(Er*Y*)Al_2		0.08	INS	12
(Er*La*)Al_2		0.12	INS	12
(Er*Sc*)Al_2		0.08	INS	12

cluster coexists with the fine structure as an intermediate step, because with our interpretation intensity builds at the center of the spectrum. Finally, the whole structure narrows. It is clearly reasonable to explain the 2500-ppm (Er*Y*)Al_2 data in exactly the same way except the first low-temperature set of data is not available in this case. It would be interesting to follow the 500-ppm sample to higher (>4.2 K) temperatures where it might be expected to narrow. This is impractical at present because of the rapidly reducing signal strength for higher temperatures. This conventional way of treating interacting resonances in the EPR of dilute alloys as a phenomenological cluster line is not in conflict with a more microscopic point of view, namely, the analysis in terms of spin pairs and triplets, etc., such as in insulators.

VI. SUMMARY

The present paper discusses the Γ_8 resonance of Er in YAl_2 single crystals. Details of the experimental and fit procedure are presented as well as theoretical calculations on the relaxation rates. We will summarize firstly the CEF parameters, secondly the g-value shift and Korringa rates, and finally the anisotropic exchange.

A full citation of the experimental work of x and W in $(Er_cY_{1-c})Al_2$ goes beyond the scope of this paper. In Table II we have selected some data. These and a careful analysis of others (see references in Refs. 4, 12, 16, and 29) lead us to the conclusion that x and W do not change systematically with concentration from $c=100\%$ to 500 ppm. x and W remain almost constant. The reason for different suggestions in the literature may concern a very technical point.[6] One could argue that the electron concentration or band structure does vary systematically as a function of concentration.[13] The conclusion of the present work is that it does not—at least it does not manifest such variation in a systematic change of A_4 and A_6 (respectively x and W). 100% $ErAl_2$ (Ref. 19) yields in the magnetization almost the same CEF as in the present work, provided the internal field in the ferromagnetic phase is taken properly into the analysis. We have calculated the energy levels of the $\Gamma_8^{(3)}$ and $\Gamma_8^{(2)}$ as a function of magnetic field up to 60 kG. According to Eqs. (1) and (2) and fixed x and W the energy scheme changes completely. A crossover for the levels 3 and 4 as well as 5 and 6 happens, that is to say, the center of gravity for the $\Gamma_8^{(3)}$ and $\Gamma_8^{(2)}$ changes.[42]

Consequently some INS experiments with poor energy resolution may have determined an incorrect energy separation for the levels. If, however, our

TABLE IV. Anisotropic exchange constants for different hosts. The parameters are determined with respect to Eq. (3). Most data are a reanalyzation of previously published experimental results.

System	x	W(K)	$N(E_F)J_0$	$N(E_F)J_4$	$N(E_F)J_6$	Ref.
Dy*Pd*	−0.422	−0.092	−0.206	$+3\times10^{-3}$	-4.37×10^{-6}	26,27,28
Dy*Pd*	−0.559	−0.17	−0.235	$+2.86\times10^{-6}$	$+6.3\times10^{-7}$	26,27
Er*Pd*	+ 0.457	−0.16	−0.235	$+2.86\times10^{-6}$	$+2.08\times10^{-7}$	26,29,30
Dy*Pt*	+ 0.7625	+ 0.124	−0.071	-2.1×10^{-5}	$+4.1\times10^{-7}$	26
Er*Pt*	−0.769	+ 0.085	−0.071	-2.1×10^{-5}	$+8.3\times10^{-7}$	7,26
(Er*Y*)Al_2	−0.322	−0.29	+ 0.09	$\pm5\times10^{-5}$	$\pm6\times10^{-8}$	This work

conclusion is correct, namely, that replacing an yttrium ion by an erbium ion does not change the electron concentration and the CEF, respectively, very much, one has to argue that it should be roughly the same situation for Er in $ScAl_2$. Indeed, we have measured 500-ppm Er in a $ScAl_2$ single crystal, and again we find a $\Gamma_8^{(3)}$ resonance. This is in conflict with previous work[13] but in perfect agreement with the most recent INS work.[12]

In Table III we summarize the g-value shift and relaxation date. The determination of these parameters highly depends on the assumption of the CEF ground state. In our previous work[14] the x, W values are incorrect as is the g-value shift (second row in Table III). Moreover, if one assumes a Γ_7 ground state and strong concentration-dependent CEF levels, as discussed in the preceding paragraph, the g-value shift $N(E_F)J^{\Delta g}$ will exhibit the same pseudodependence. A theoretical analysis employing partial wave analysis of the exchange integral and partial density of states[13] is certainly not any more solidly based on experimental ground. From the first and third line of Table III we follow that the exchange coupling of Gd and Er to the conduction electrons is almost the same. This result is not surprising. A similar situation exists for Gd*Au* (Ref. 38) and Er*Au* (Ref. 24). A significant change occurs if we turn to Pt and Pd as a host (Table IV). These are the only host matrices known to date where Er exhibits a strong negative g-value shift. The analysis of the angle-dependent resonance field also yields contributions to the anisotropic exchange, which are significantly larger than in the present work and out of experimental uncertainties. The question arises as to why Pt and Pd are different than any other host, i.e., Au, Al, YAl_2, etc. One possible interpretation is strong covalency, as discussed in Sec. III. This point needs further investigation.

A comparison between the experimental techniques INS and ESR in Table III shows that the static local susceptibility as determined by the g-value shift cannot be detected by INS. The dynamic contribution of the exchange interaction can be detected by both techniques equally. However, the error bar in INS is larger due to the larger linewidth. More details of the dynamics of impurity-impurity interactions, as we have discussed in Sec. V for the first time in a Γ_8 resonance, are not visible in the INS experiment. For the system in question, Er in cubic Laves phases, both techniques yield very consistent and reliable results.

ACKNOWLEDGMENTS

We acknowledge fruitful discussions with M. Loewenhaupt during various stages of the work. We thank D. Shaltiel for discussions and E. Tsang for help in the sample preparation. This work was supported by Deutsche Forschungsgemeinschaft (Sondersforschungsbereich 161).

[1]K. W. H. Stevens, Proc. Phys. Soc. London, Sect. A 65, 209 (1952).

[2]For notation and symbols see also A. Abragam and B. Bleaney, *EPR of Transition Ions* (Clarendon, Oxford, 1970).

[3]K. R. Lea, M. J. M. Leask, and W. P. Wolf, J. Phys. Chem. Solids 23, 1381 (1962).

[4]See (a) *Proceedings of the International Crystalline Electric Field Conference II, Crystal Field Effects in Metals and Alloys,* edited by A. Furrer (Plenum, New York, 1976); (b) *Proceedings of the International Crystalline Electric Field Conference III, Crystalline Electric Field and Structural Effects in f-Electron Systems,* edited by J. E. Crow, R. P. Guertin, and T. W. Mihalisin (Plenum, New York, 1979); (c) *Proceedings of the International Crystalline Electric Field Conference IV, International Conference on Crystal Field and Structual Effects in f-Electron Systems,* edited by R. P. Guertin, W. Suski, and Z. Zotnierek (Plenum, New York, 1982).

[5]K. W. H. Stevens, Ref. 4(b), p. 1.

[6]K. Baberschke, in Ref. 4(c), p. 101.

[7]S. E. Barnes, Adv. Phys. 30, 801 (1981).

[8]K. Baberschke, B. Bachor, and S. E. Barnes, Phys. Rev. B 21, 2666 (1980).

[9]A. Fert and P. M. Levy, Phys. Rev. B 16, 5052 (1977).

[10]N. L. Huang Liu, K. J. Ling, and R. Orbach, Phys. Rev. B 14, 4087 (1976); N. L. Huang Liu and R. Orbach, *ibid.* 17, 3701 (1978).

[11]See various contributions in Ref. 4

[12]M. Loewenhaupt, S. Horn, and B. Frick, in Ref. 4(c), p. 125.

[13]R. A. B. Devine, W. Zingg, J. H. Moret, and D. Shaltiel, Solid State Commun. 12, 515 (1973); R. A. B. Devine, M. Poirier, and T. Cyr, J. Phys. F 5, 1407 (1975).

[14]K. Baberschke, B. Bachor, H. Luft, and J. Pellisson, J. Phys. (Paris) Colloq. C5, 51 (1979).

[15]H. E. Hoenig and R. Voitmann, Solid State Commun. 33, 43 (1980).

[16]R. Levin, A. Grayevsky, D. Shaltiel, and V. Zevin, Solid State Commun. 37, 69 (1981).

[17]J. G. Sereni, in Ref. 4(a), p. 309.

[18]H. Heer, A. Furrer, E. Walker, A. Treyrand, H. G. Purwins, and J. Kjems, J. Phys. (Paris) Colloq. C7, 1207 (1974).

[19]H. G. Purwins, E. Walker, B. Barbara, M. F. Rossignol, and A. Furrer, J. Phys. C 9, 1025 (1976).

[20]H. Happel, P. V. Blanckenhagen, H. Knorr, and A. Murani, in Ref. 4(a); P. Blanckenhagen, H. Happel, and H. Knorr, J. Magn. Magn. Mater. 9, 20 (1978).
[21]M. Loewenhaupt, K. Baberschke, and H. Scheuer, Solid State Commun. 33, 175 (1980).
[22]U. Walter and E. Holland-Moritz, Z. Phys. B 45, 107 (1981).
[23]J. M. Baker and R. L. Wood, Bull. Magn. Resonance 2, 149 (1981).
[24]Y. V. Spalden and K. Baberschke, J. Magn. Magn. Mater. 23, 183 (1981).
[25]J. Czrochalski, Z. Phys. Chem. 92, 219 (1918).
[26]J. Pellisson, Thèse, Universite de Genève, 1977 (unpublished).
[27]R. A. B. Devine, J. M. Moret, J. Ortelli, D. Shaltiel, W. Zingg, and M. Peter, Solid State Commun. 10, 575 (1972).
[28]Y. Yang, N. L. Huang Liu, and R. Orbach, Solid State Commun. 18, 1443 (1976).
[29]R. A. B. Devine, W. Zingg, and J. M. Moret, Solid State Commun. 11, 233 (1972).
[30]W. Zingg, H. Bill, J. Buttet, and M. Peter, Phys. Rev. Lett. 32, 1221 (1974).
[31]In the literature one finds occasionally $L=(2-g_J)J$. This is not correct in our case.
[32]H. K. Sy and M. B. Walker, J. Phys. F 5, 1064 (1975).
[33]M. Hardiman, J. Pellisson, S. E. Barnes, P. E. Bisson, and M. Peter, Phys. Rev. B 22, 2175 (1980).
[34]J. J. Tao, D. Davidov, R. Orbach, and E. P. Chock, Phys. Rev. B 4, 5 (1971).
[35]A change in the mixture of absorption and dispersion does not influence the linewidth parameter but changes dramatically H_{res}. See, e.g., M. Peter, D. Shaltiel, J. H. Wernick, H. J. Williams, J. B. Mock, and R. C. Sherwood, Phys. Rev. 126, 1395 (1962).
[36]For the purpose of discussion we use first an exchange Hamiltonian as common in the literature and not Eq. (3). At the end of this section we discuss precisely Eq. (3) and replace $J^{\Delta g}$ by J_0.
[37]Note that the intensity in a metal resonance is proportional to $(\Delta H)^2$.
[38]Due to the different curvature of $E(H)$ in Fig. 2.
[39]K. Baberschke and Y. V. Spalden, Phys. Rev. B 19, 5933 (1979).
[40]M. Zomack, K. Baberschke, and S. E. Barnes, Phys. Rev. B 27, 4135 (1983).
[41]P. Urban, D. Davidov, B. Elschner, T. Plefka, and G. Sperlich, Phys. Rev. B 12, 72 (1975).
[42]U. Döbler, Diplomarbeit, Freie Universität Berlin, 1982 (unpublished).
[43]C. Rettori, P. Davidov, G. Ng, and E. P. Chock, Phys. Rev. B 12, 1298 (1975).